Supplementary Material

1 CHEMTEX-derived phytoplankton composition

CHEMTAX analysis was performed using HPLC-measured pigment concentrations as the input to derive the composition of the major phytoplankton groups within each water sample. Since there have been no previous CHEMTAX based estimates of phytoplankton groups from the uGoT, the initial pigment ratios used in CHEMTAX were those from studies in the East China Sea (Xu et al., 2019) and central Bohai Sea (Lu et al., 2018) and the experimental study on pigment changes during the evolution of green *Noctiluca* in the Gulf of Thailand (Furuya and Lirdwitayaprasit, 2000). The CHEMTAX program was subsequently run fifteen times using the HPLC data separately for each cruise. The output ratio matrix of the last run was used as the next ratio matrix input, and finally output of the most stable ratio among the fifteen-times runs was selected as the phytoplankton composition used in this study (Latasa, 2007). The calculation was done separately for each observation: NOM2017, SWM2018, NEM2018, and SWM2019. Matrices of the initial and final pigment ratios are summarized in Table S1.

Table S1. Initial and final ratios of pigments to chl-a for the eight phytoplankton groups used in the CHEMTAX analysis.

Taxonomic group/ Pigment	Peridinin	19Butfu	Fucoxanthin	19Hexfu	Alloxanthin	Neoxanthin	Violaxanthin	Zeaxanthin	Lutein	chlorophyll-b	Chlorophyll-a	Reference
Initial ratio												
Dinoflagellates	1.062	0	0	0	0	0	0	0	0	0	1	Lu et al. 2018
Cryptophytes	0	0	0	0	0.14	0	0	0	0	0	1	Xu et al. 2019
Prymnesiophytes	0	0	0	1.4	0	0	0	0	0	0	1	Xu et al. 2019
Haptophytes (T4)	0	0.246	0.585	0.538	0	0	0	0	0	0	1	Lu et al. 2018
Cyanobacteria	0	0	0	0	0	0	0	0.35	0	0	1	Lu et al. 2018
Diatoms	0	0	0.75	0	0	0	0	0	0	0	1	Lu et al. 2018; Xu et al. 2019
Chlorophyte: exponential phase	0	0	0	0	0	0.08	0.118	0.059	0.224	0.092	1	Furuya and Lirdwitayaprasit 2000
Cholrophyte: stationary phase	0	0	0	0	0	0.132	0.194	0.244	0.477	0.088	1	Furuya and Lirdwitayaprasit 2000
Final ratio (NEM 2017)												
Dinoflagellates	0.735	0	0	0	0	0	0	0	0	0	1	
Cryptophytes	0	0	0	0	0.06	0	0	0	0	0	1	
Prymnesiophytes	0	0	0	1.4	0	0	0	0	0	0	1	
Haptophytes (T4)	0	0.262	0.327	0.538	0	0	0	0	0	0	1	
Cyanobacteria	0	0	0	0	0	0	0	0.013	0	0	1	
Diatoms	0	0	0.336	0	0	0	0	0	0	0	1	
Chlorophyte: exponential phase	0	0	0	0	0	0.013	0.007	0.050	0.005	1.458	1	
Cholrophyte: stationary phase	0	0	0	0	0	0.084	0.053	8.287	0.072	0.088	1	
Final ratio (SWM 2018)												
Dinoflagellates	0.811	0	0	0	0	0	0	0	0	0	1	
Cryptophytes	0	0	0	0	0.01	0	0	0	0	0	1	
Prymnesiophytes	0	0	0	1.4	0	0	0	0	0	0	1	
Haptophytes (T4)	0	0.246	0.585	0.538	0	0	0	0	0	0	1	
Cyanobacteria	0	0	0	0	0	0	0	0.649	0	0	1	
Diatoms	0	0	0.475	0	0	0	0	0	0	0	1	
Chlorophyte: exponential phase	0	0	0	0	0	0.016	0.008	0.003	0.057	0.721	1	
Cholrophyte: stationary phase	0	0	0	0	0	0.150	0.138	0.007	0.824	0.089	1	
Final ratio (NEM 2018)												
Dinoflagellates	0.496	0	0	0	0	0	0	0	0	0	1	
Cryptophytes	0	0	0	0	0.14	0	0	0	0	0	1	
Prymnesiophytes	0	0	0	1.4	0	0	0	0	0	0	1	
Haptophytes (T4)	0	0.246	0.585	0.538	0	0	0	0	0	0	1	
Cyanobacteria	0	0	0	0	0	0	0	0.002	0	0	1	
Diatoms	0	0	0.636	0	0	0	0	0	0	0	1	
Chlorophyte: exponential phase	0	0	0	0	0	0.014	0.015	0.061	0.016	2.233	1	
Cholrophyte: stationary phase	0	0	0	0	0	0.039	0.033	1.764	0.079	0.075	1	
Final ratio (SWM 2019)												
Dinoflagellates	0.401	0	0	0	0	0	0	0	0	0	1	
Cryptophytes	0	0	0	0	0.287	0	0	0	0	0	1	
Prymnesiophytes	0	0	0	1.4	0	0	0	0	0	0	1	
Haptophytes (T4)	0	0.246	0.585	0.538	0	0	0	0	0	0	1	
Cyanobacteria	0	0	0	0	0	0	0	0.335	0	0	1	
Diatoms	0	0	0.233	0	0	0	0	0	0	0	1	
Chlorophyte: exponential phase	0	0	0	0	0	0.020	0.014	0.002	0.086	0.404	1	
Cholrophyte: stationary phase	0	0	0	0	0	0.173	0.193	0.219	0.886	0.115	1	

Note: 19Butfu and 19Haxfu are 19′-butanoyloxyfucoxanthin and 19′-hexanoyloxyfucoxanthin, respectively.

2 RAMSES hyperspectral radiometer measurement

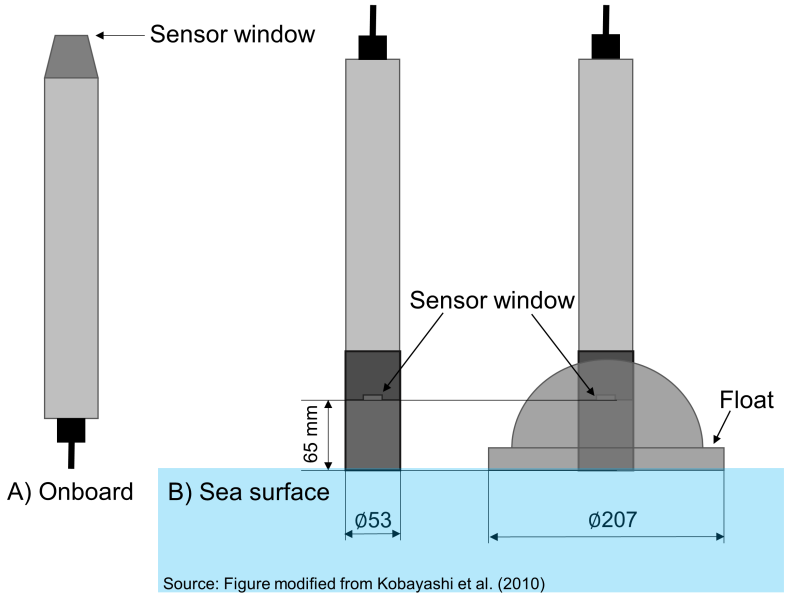

Figure S1. Schematic diagram of RAMSES hyperspectral radiometer measurement: one onboard sensor measuring sky irradiance (A) and two sensors measuring water-leaving radiance just above the sea surface (B). The radiance sensors in (B) are covered by different sizes of domes to correct the self-shading (Kobayashi et al., 2010).

3 Correction of MODIS remote sensing reflectance (R_{rs}) and R_{rs} ratios

This supplementary section showed the correction of MODIS remote sensing reflectance (R_{rs}) and R_{rs} ratio over the upper Gulf of Thailand (Figure S2) based on the match-up methods in Luang-on et al. (2021) using 49 datasets obtained from their study and 9 new datasets from our observation. This study defined satellite match-ups as the median of valid R_{rs} data (at least one pixel) within a 3x3 box of the pixel center acquired within $\pm$24 hour time difference from the shipboard sampling. The quality of each valid pixel was controlled by the masks LAND, HIGLINT, HILT, CLDICE, HISOLZEN, LOWLW, CHLFAIL, and NAVFAIL. The percentage root-mean-square error (RMSE, %) and the percentage bias (Bias, %) were used to evaluate the performance of R_{rs} and R_{rs} ratio from MODIS and *in situ* sensors (Campbell and O'Reilly, 2006). The statistical equations are as follows:

$$RMSE(\%) = 100 \times \sqrt{\frac{1}{N}\sum_{i=1}^{N}\left(\frac{X_{modis}-X_{obs}}{X_{obs}}\right)^2},$$

$$Bias(\%) = 100 \times \frac{1}{N}\sum_{i=1}^{N}\frac{X_{modis}-X_{obs}}{X_{obs}},$$

where X_{modis} and X_{obs} are MODIS and *in situ* R_{rs}, respectively, and N is the number of data.

Comparison of *in situ* and MODIS ratio of $R_{rs}488/R_{rs}547$ showed strong correlation implying no serious atmospheric correction problem over the uGoT (Luang-on et al., 2021, Figure S3A), whereas MODIS ratios of $R_{rs}531/R_{rs}547$ and $R_{rs}667/R_{rs}547$ demonstrated overestimation and

underestimation, respectively (Figure S3B-C). Two steps of MODIS R_{rs} correction were thus performed for the single R_{rs} data (Figure S4) and R_{rs} ratios (Figure S5) to minimize the errors.

For single MODIS R_{rs}, Hayashi et al. (2015) developed a R_{rs} correction method based on the linear relationship between *in situ* $R_{rs}412$ and $R_{rs}547$ nm for correcting underestimation in MODIS R_{rs} at shorter wavelengths than 547 nm. The method has also been applied to corrected MODIS R_{rs} errors in overestimation as well as underestimation of $R_{rs}412$ by Yang et al. (2018). We only applied this method to correct the underestimated $R_{rs}488$ and $R_{rs}531$ when $R_{rs}412$ is negative (Figure S4A-D). Using the corrected R_{rs} to be normalized by $R_{rs}547$ (Figure S4E-F), the correlation of *in situ* and MODIS data slightly improved for $R_{rs}488/R_{rs}547$ (R^2 from 0.90 to 0.93) and $R_{rs}531/R_{rs}547$ (R^2 from 0.86 to 0.90).

For MODIS R_{rs} ratios, the overestimation and underestimation of MODIS data were found in the ratios of $R_{rs}531/R_{rs}547$ and $R_{rs}667/R_{rs}547$, respectively (Figure S3B, C, and S4F). Therefore, a linear relationship between *in situ* and satellite R_{rs} ratio based on reduced major axis regression were investigated (Fig. S5A, C) and applied to correct the errors of $R_{rs}531/R_{rs}547$ and $R_{rs}667/R_{rs}547$ (Figure S5B, D). The accuracy of MODIS data showed a marked improvement over the corrected R_{rs} ratios (bias from 5.857% to 0.102% for $R_{rs}531/R_{rs}547$ and from -30.980% to 8.956% for $R_{rs}667/R_{rs}547$).

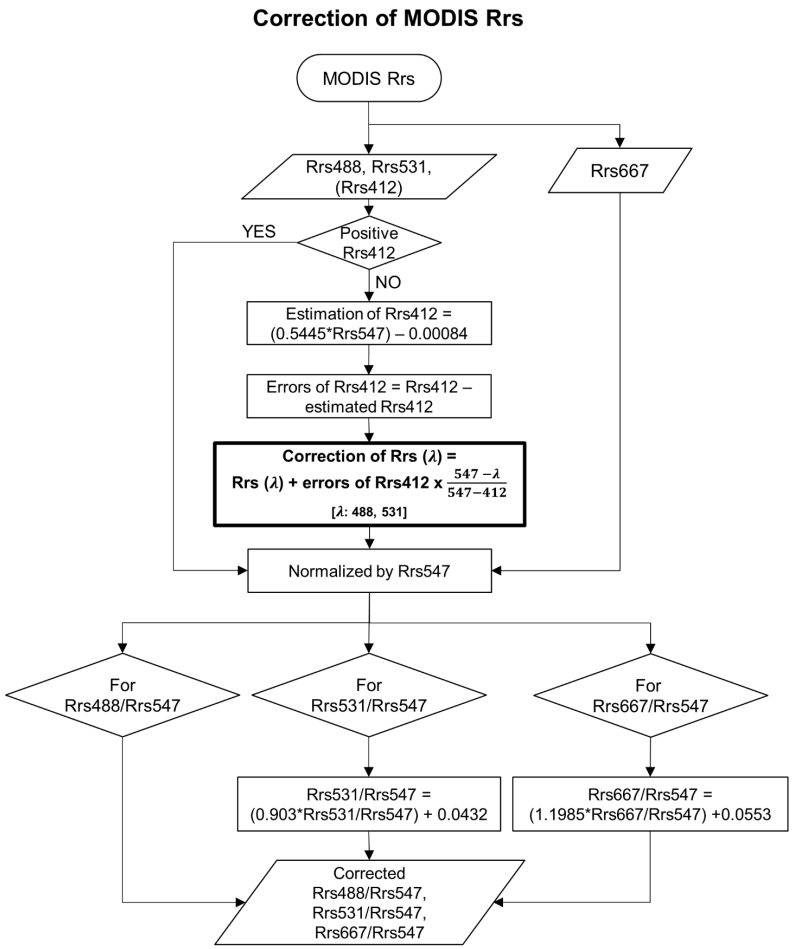

Figure S2. Process flow diagram of linear correction of MODIS data.

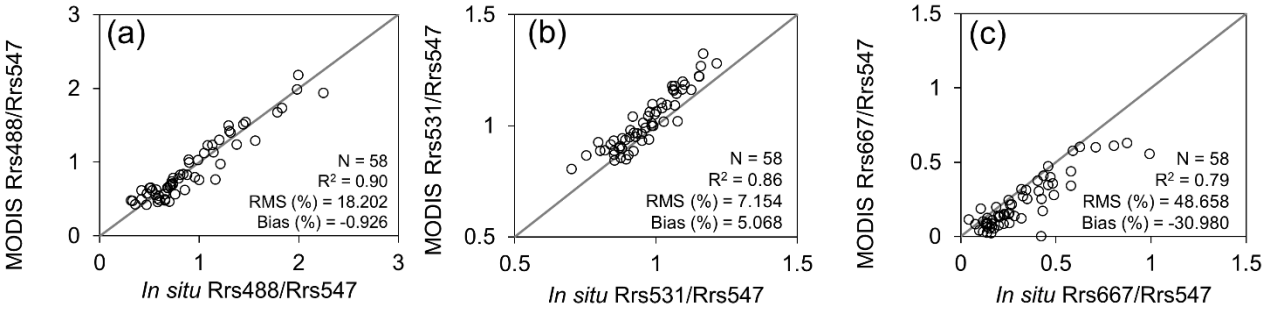

Figure S3. Comparison of *in situ* and MODIS R_{rs} ratios of $R_{rs}488/R_{rs}547$ (A), $R_{rs}531/R_{rs}547$ (B), and $R_{rs}667/R_{rs}547$ (C) before MODIS R_{rs} correction.

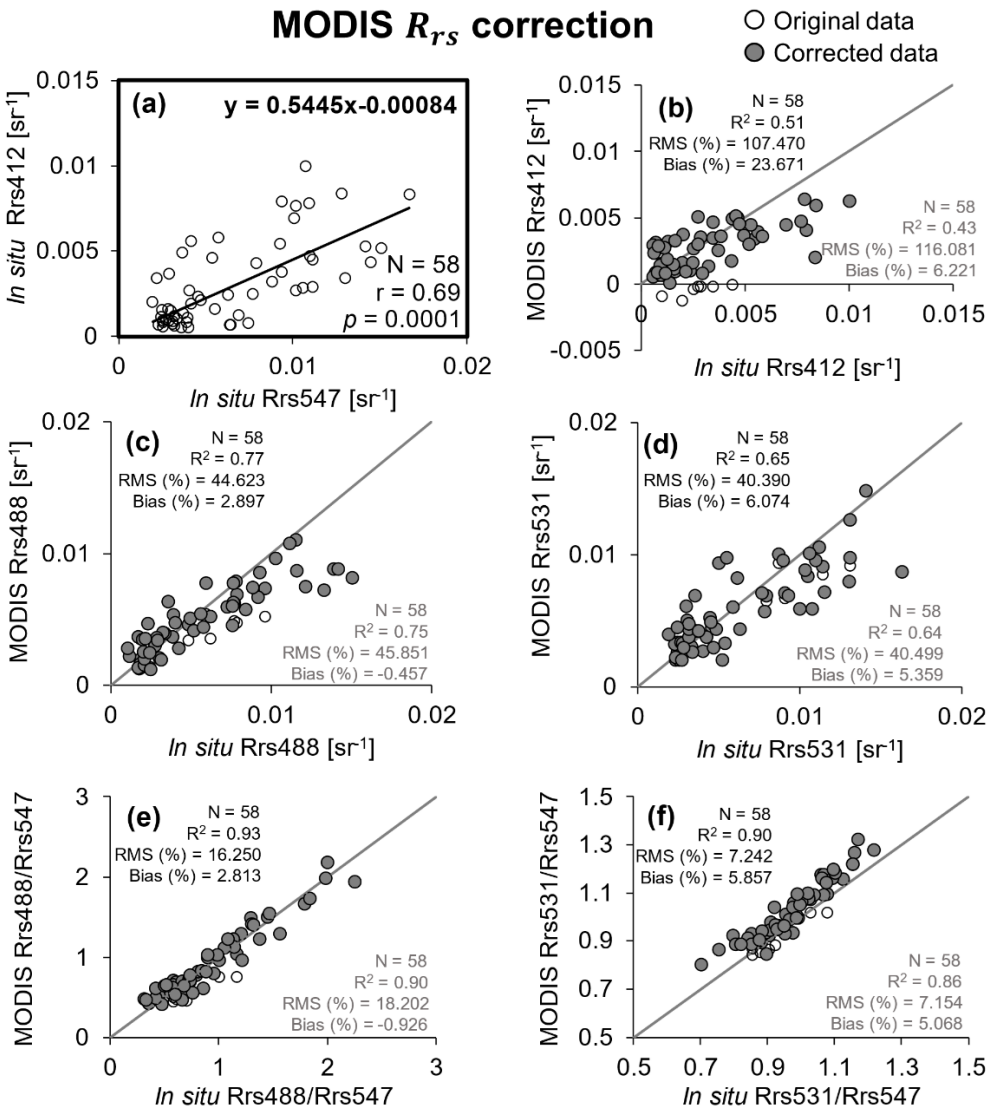

Figure S4. Comparison of *in situ* $R_{rs}412$ and $R_{rs}547$ (A), *in situ* and MODIS in the single wavelengths of $R_{rs}412$ (B), $R_{rs}488$ (C), and $R_{rs}531$ (D), and ratios of $R_{rs}488/R_{rs}547$ (E) and $R_{rs}531/R_{rs}547$ (F). Grey and hollow circles in (B)-(F) are the data before and after correction, respectively.

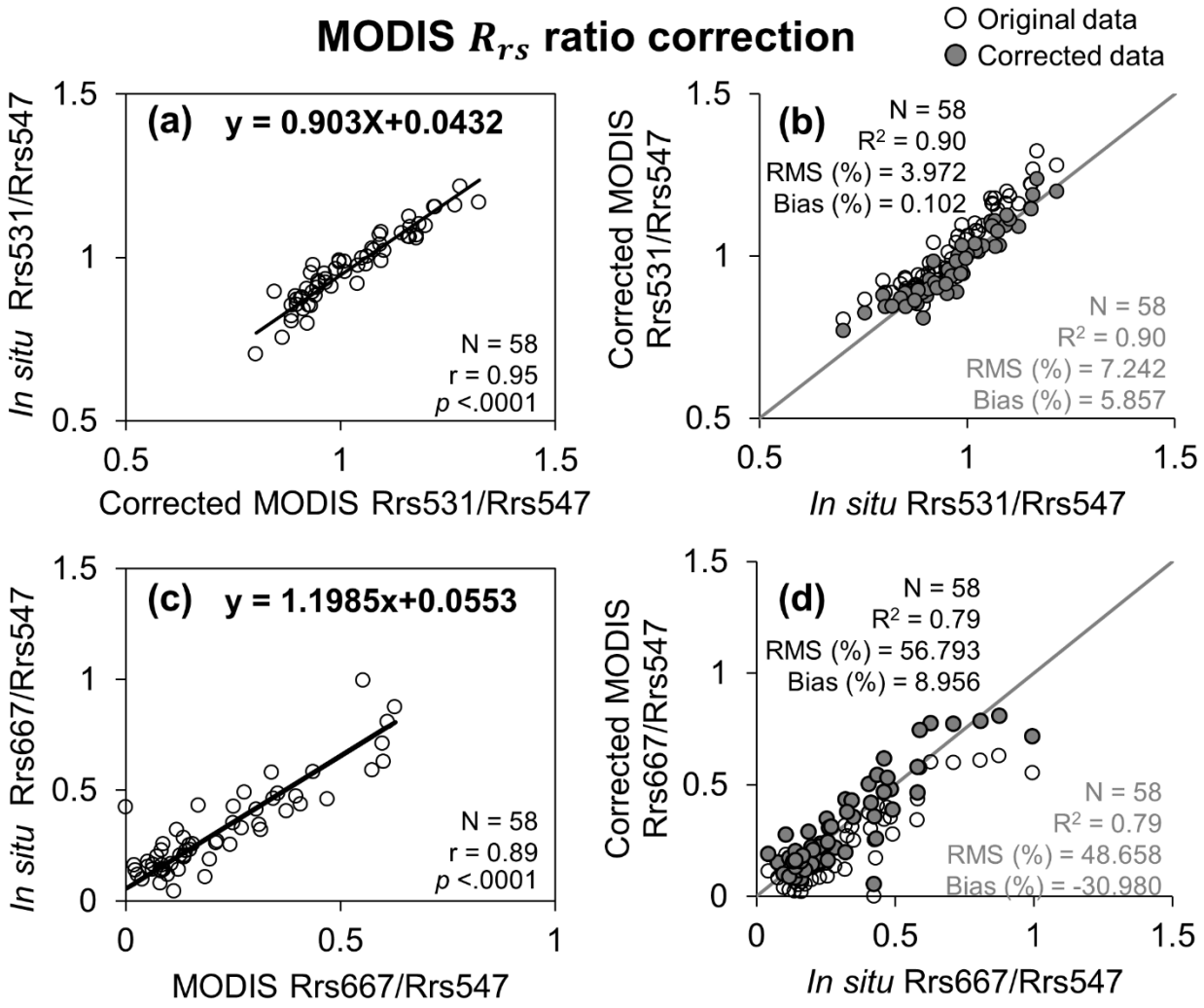

Figure S5. Comparisons of *in situ* and MODIS R_{rs} ratios of $R_{rs}531/R_{rs}547$ (A-B) and $R_{rs}667/R_{rs}547$ (C-D). Grey circles in (B) and (D) are the MODIS data before correction. Hollow circles in (B) and (D) are the estimated MODIS data using linear functions in (A) and (C), respectively.

4 Reference

Campbell, J. W., and O'Reilly, J. E. (2006). Metrics for Quantifying the Uncertainty in a Chlorophyll Algorithm: Explicit equations and examples using the OC4.v4 algorithm and NOMAD data. Available at: https://oceancolor.gsfc.nasa.gov/meetings/ocbam/PerformanceMetrics.pdf.

Furuya, K., and Lirdwitayaprasit, T. (2000). Pigment composition of Pedinomonas noctilucae (Pedinophyceae), an endosymbiont of green Noctiluca (Dinophyceae). *La mer* 38, 95–97.

Hayashi, M., Toratani, M., Kobayashi, H., Maekawa, Y., Nakamura, T., Nakashima, Y., et al. (2015). Seasonal and Inter-annual Variability of Satellite Chlorophyll-a in Ise-Mikawa Bay.

Kobayashi, H., Ishizaka, J., Jintasaeranee, P., Gunbua, Vi., and Fukasawa, T. (2010). Water-Leaving Radiance Measured Using with Covered Radiometers in Highly Turbid Waters. in *In Proceedings of the Ocean Optics XX, Anchorage, AK, USA, 27 September–1 October 2010* (Anchorage, AK, USA).

Latasa, M. (2007). Improving estimations of phytoplankton class abundances using CHEMTAX. *Mar Ecol Prog Ser* 329, 13–21. doi: 10.3354/meps329013.

Lu, L., Jiang, T., Xu, Y., Zheng, Y., Chen, B., Cui, Z., et al. (2018). Succession of phytoplankton functional groups from spring to early summer in the central Bohai Sea using HPLC–CHEMTAX approaches. *J Oceanogr* 74, 381–392. doi: 10.1007/s10872-018-0469-x.

Luang-on, J., Ishizaka, J., Buranapratheprat, A., Phaksopa, J., Goes, J. I., Kobayashi, H., et al. (2021). Seasonal and interannual variations of MODIS Aqua chlorophyll-a (2003–2017) in the Upper Gulf of Thailand influenced by Asian monsoons. *J Oceanogr*. doi: 10.1007/s10872-021-00625-2.

Xu, Q., Sukigara, C., Goes, J. I., Gomes, R., Zhu, Y., and Wang, S. (2019). Interannual changes in summer phytoplankton community composition in relation to water mass variability in the East China Sea. *J Oceanogr* 75, 61–79. doi: 10.1007/s10872-018-0484-y.

Yang, M. M., Ishizaka, J., Goes, J. I., Gomes, H. do R., Maúre, E. de R., Hayashi, M., et al. (2018). Improved MODIS-Aqua chlorophyll-a retrievals in the turbid semi-enclosed Ariake Bay, Japan. *Remote Sens (Basel)* 10, 1335. doi: 10.3390/rs10091335.